

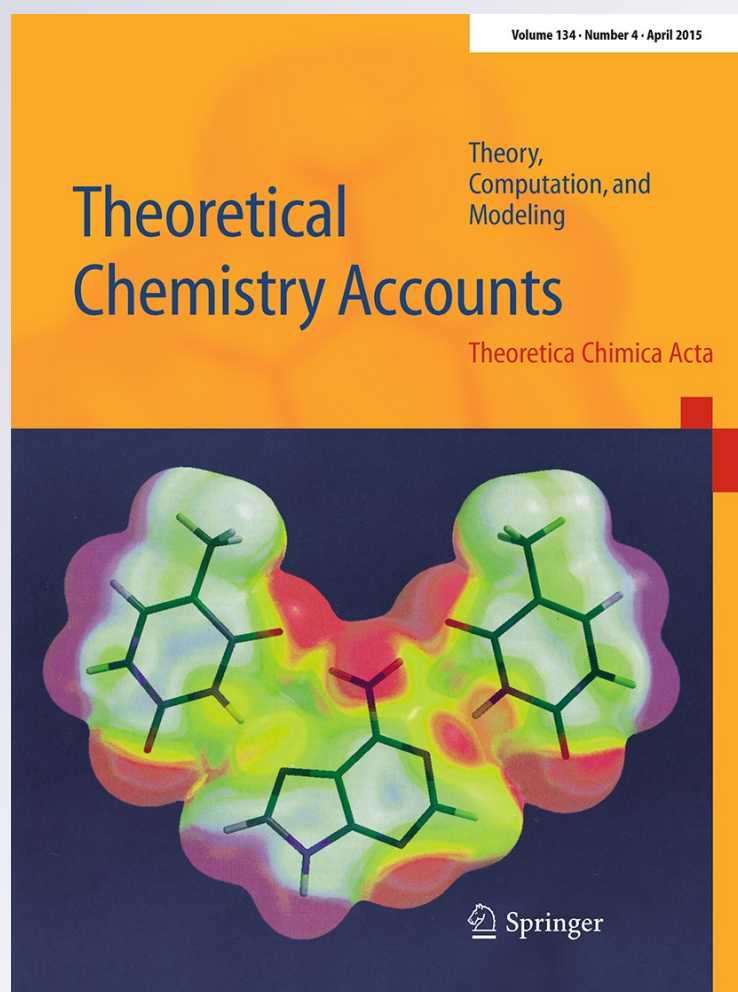
Electronic effects on the reaction mechanism of the metalloenzyme peptide deformylase

Jason S. Fell, Darren M. Steele, Tommy C. Hatcher & Benjamin F. Gherman

Theoretical Chemistry Accounts
Theory, Computation, and Modeling

ISSN 1432-881X
Volume 134
Number 5

Theor Chem Acc (2015) 134:1-7
DOI 10.1007/s00214-015-1674-y



 Springer

Your article is protected by copyright and all rights are held exclusively by Springer-Verlag Berlin Heidelberg. This e-offprint is for personal use only and shall not be self-archived in electronic repositories. If you wish to self-archive your article, please use the accepted manuscript version for posting on your own website. You may further deposit the accepted manuscript version in any repository, provided it is only made publicly available 12 months after official publication or later and provided acknowledgement is given to the original source of publication and a link is inserted to the published article on Springer's website. The link must be accompanied by the following text: "The final publication is available at link.springer.com".

Electronic effects on the reaction mechanism of the metalloenzyme peptide deformylase

Jason S. Fell¹ · Darren M. Steele¹ · Tommy C. Hatcher III¹ · Benjamin F. Gherman¹

Received: 13 November 2014 / Accepted: 27 April 2015
© Springer-Verlag Berlin Heidelberg 2015

Abstract The metalloenzyme peptide deformylase (PDF) plays a crucial role in the biosynthesis of proteins by eubacteria, making the enzyme a promising target for anti-bacterial agents. In a reaction catalyzed by an Fe(II) coordination complex in the enzyme active site, PDF cleaves a formyl group from the N-terminus of nascent eubacterial proteins. Computational chemistry methods are combined with the use of *in silico* models of the enzyme chemistry to examine specific effects on the enzymatic catalysis. In particular, density functional theory calculations have been carried out on a biomimetic model system based on a heteroscorpionate $N_2S_{thiolate}$ biomimetic ligand system bearing a range of electron-donating and electron-withdrawing substituents. In this way, the effects of electronic changes to the metal coordination environment on the thermodynamics and kinetics of the deacylation reaction are determined. The reaction was found to be more thermodynamically favorable as the added substituents shifted from electron-withdrawing to electron-donating [or, equivalently, with decreasing Hammett parameters (σ_p) for the substituents]. As the substituents change from electron-withdrawing to electron-donating, the hydroxide ligand responsible for initiating nucleophilic attack on the carbonyl group of the formyl-terminated peptide substrate is shown to become decreasingly strongly bound to the metal, making the

reaction less endergonic. The rate of reaction was found to be fastest for substituents with $\sigma_p \approx 0$, and progressively slower as the substituents became increasingly electron-donating or electron-withdrawing. At $\sigma_p \approx 0$, a balance is found between the reactivity of the hydroxide ligand involved in the nucleophilic attack and activation of the carbonyl group by the iron center toward that nucleophilic attack.

Keywords Peptide deformylase · Substituent effects · Density functional calculations · Reaction thermodynamics and kinetics · Metalloenzymes

1 Introduction

The metalloenzyme peptide deformylase (PDF) catalyzes the N-terminal deacylation of newly synthesized peptides during eubacterial protein biosynthesis [1–4]. PDF is therefore essential to the life cycle of eubacteria, and its absence from eukaryotic cells has made it a promising target for antibiotic drug design [5–9].

Crystal structures of PDF [1, 10] have indicated the structure of the enzyme's active site and led to a proposed mechanism for the deacylation reaction. The active site consists of an Fe^{II} metal center coordinated to the side chains of two histidine residues (His132 and His136) and one deprotonated cysteine residue (Cys90). A hydroxide ion fills a fourth coordination spot around the metal center, giving an approximately tetrahedral coordination complex. The reaction mechanism [10] (Fig. 1) begins with the carbonyl carbon on the formyl-terminated peptide undergoing nucleophilic attack by the hydroxide ligand. Weak coordination of the carbonyl oxygen from the terminal amide group of the peptide to the iron center (i.e., the metal

Electronic supplementary material The online version of this article (doi:10.1007/s00214-015-1674-y) contains supplementary material, which is available to authorized users.

✉ Benjamin F. Gherman
ghermanb@csus.edu

¹ Department of Chemistry, California State University, Sacramento, 6000 J Street, Sacramento, CA 95819-6057, USA

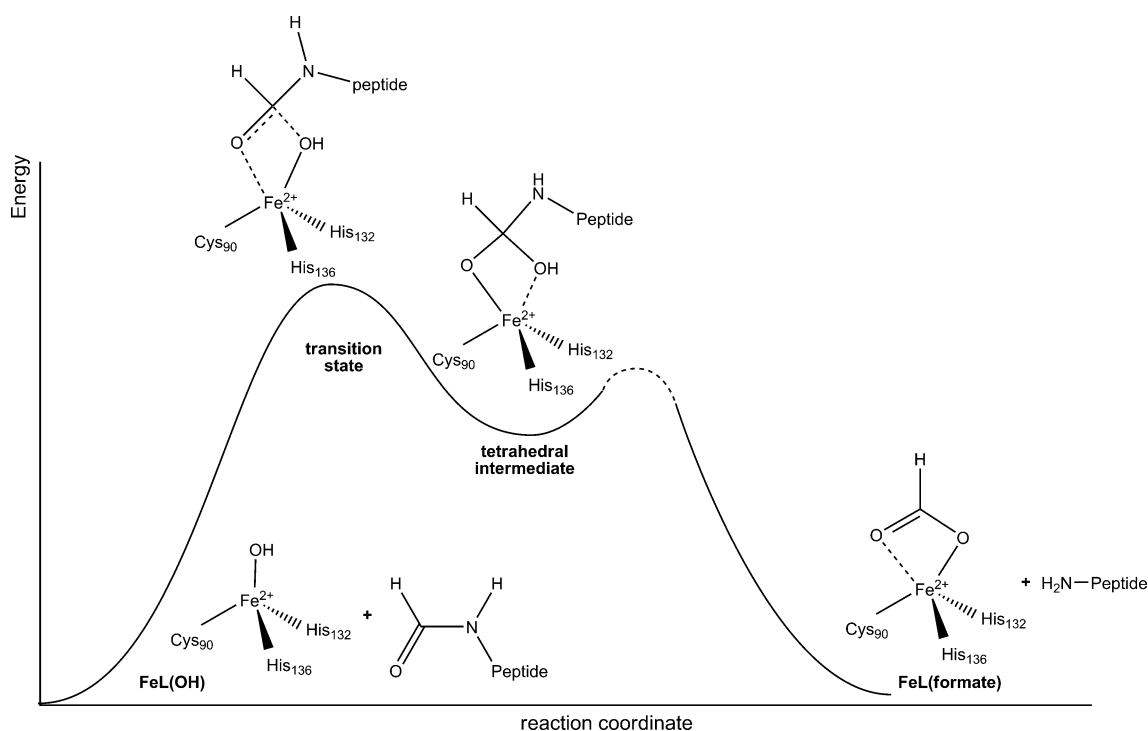


Fig. 1 Proposed mechanism for the deformylation reaction catalyzed by PDF, with active site residues indicated

center acting as a Lewis acid) helps to activate the substrate toward the nucleophilic attack. Following the nucleophilic attack, a tetrahedral intermediate is formed. Proton transfers then lead to release of the deformylated peptide and formation of an enzyme–formate complex. Comparison with the crystal structures of PDF with Ni^{II} suggested the importance of the relative softness of the Fe^{II} metal center, which would then weakly bind the hard base OH^- , leading to a relatively high nucleophilicity for the Fe-OH group [11].

Past computational studies on the PDF enzyme have included active site modeling [12] and QM/MM calculations [13–15]. In both cases, the structures of stationary points involved in the catalytic mechanism and energetics along the reaction coordinate were examined, in order to address the preference for Fe^{II} as the active site metal ion (versus, for example, Zn^{II} , Co^{II} , or Ni^{II}) [3, 16], despite Fe^{II} being uncommon for this class of metalloenzymes [17] and that PDF catalyzes a non-redox reaction. It was determined that Fe^{II} led to the lowest activation barriers for nucleophilic attack due to the ability of Fe^{II} to act as a Lewis acid and thereby to more strongly coordinate to and activate the substrate carbonyl leading to a decrease in the energy barrier for the reaction.

Further computational work followed, this time using biomimetic $\text{N}_2\text{S}_{\text{thiolate}}$ ligand systems, which model the two histidine side chains and one cysteine coordinated to Fe^{II} in PDF, such as the PATH

(2-methyl-1-[methyl-(2-pyridin-2-yl-ethyl)amino]propane-2-thiol) ligand [18] and the heteroscorpionate ligand “L” (bis(3,5-dimethyl-pyrazolyl)(1-methyl-1-sulfanylethyl) methane) [19].

The computations with the heteroscorpionate ligand “L” [19] established this model system as being particularly suitable for its fidelity with respect to reproducing important aspects of the chemistry seen with the full PDF enzyme. The overall coordination geometry for the $\text{FeL}(\text{formate})$ complex as well as the formate coordination mode to Fe and the $\text{Fe-O}(\text{formate})$ distances were consistent with the structure of the coordination geometry seen in the PDF-formate crystal structure [20]. Similar good agreement was also seen between Co^{II} - and Zn^{II} -substituted forms of the metal-L-formate complex and the correspondingly substituted forms of PDF. In addition, the difference in computed activation energies for deformylation between Fe^{II} , Co^{II} , and Zn^{II} complexes with ligand L was fully consistent with experimental kinetics data for the Fe^{II} , Co^{II} , and Zn^{II} forms of PDF [3, 10, 16, 21] as well as with the results from the earlier QM/MM computational studies [13–15]. Moreover, the relative coordinative flexibility between tetra- and pentacoordination in the Fe^{II} complexes with ligand L was also observed in the QM/MM studies.

Overall, results obtained from the biomimetic models corroborated the results obtained from the active site modeling and QM/MM computations on the PDF enzyme, confirming the fact and nature of the preference for Fe^{II} as the

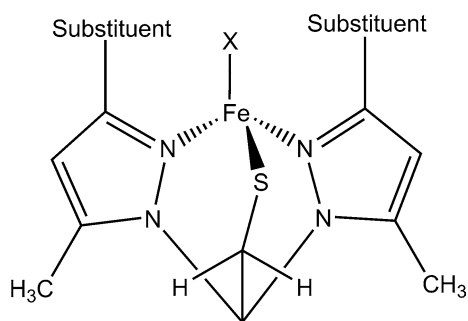


Fig. 2 Heteroscorpionate N_2S_{thiolate} biomimetic ligand (L) complexed to Fe, with substituent positions indicated

active site metal ion in PDF. Calculations with the heteroscorpionate ligand L also indicated the importance of electronic changes at the Fe^{II} center during the mechanism [19].

In short, computational work on PDF to date has indicated that the electronic characteristics of the Fe^{II} metal center are a key factor affecting the energetics of the deformylation reaction. Additionally, Brown and Gherman [19] showed that the biomimetic heteroscorpionate ligand L was an effective model for the active site of PDF. Based on this foundation, electronic effects on the deformylation reaction are probed more directly in the present work by investigating how changes in the electronic character of the biomimetic ligand L coordinating the Fe^{II} metal center affect the reaction kinetics and thermodynamics. Taking advantage that the heteroscorpionate ligand L (Fig. 2) can be readily substituted along the pyrazolyl groups [22], computations are carried out with a variety of disubstituted biomimetic ligands L, in which both substituents are varied simultaneously and identically. Substituents utilized include electron-withdrawing ($-NO_2$, $-CN$, $-CClF_2$, $-F$) and electron-donating ($-i\text{-Pr}$, $-CH_3$, $-OCH_3$, $-OCH(CH_3)_2$, $-N=CHC_6H_5$, $-NHCH_3$, $-N(CH_3)_2$) groups, with Hammett σ_p parameters¹ ranging from +0.78 (most electron-withdrawing) to -0.83 (most electron-donating) [23]. Using density functional theory (DFT) computational methods, the deformylation reaction is modeled using these disubstituted ligand systems, allowing for a determination of how reaction energies and activation energies change as a function of substituent and what factors underlie the patterns in the calculated reaction energetics.

2 Computational methods

All calculations were carried out with the Gaussian 03 (revision D.01) electronic structure program [24].

¹ Although the substituents on the biomimetic ligand L are not in a “para” position, the notation σ_p is retained as it is the Hammett σ_p parameters, which are utilized throughout this study.

Density functional theory (DFT) with the O3LYP functional [25–27] was utilized, as this method has been shown to be successful in reproducing crystal structures and metal–ligand bond lengths for coordination complexes with the heteroscorpionate ligand L [19]. The O3LYP functional also led to $FeL(\text{formate})$, $CoL(\text{formate})$, and $ZnL(\text{formate})$ structures (CH_3 substituents) [19] consistent with the coordination geometries seen in PDF-formate crystal structures [20]. The 6-31G(d,p) basis set (with the exception of the Stuttgart effective core potential basis set on the metal center [28]) was used for geometry optimizations and transition state searches. Vibrational frequency calculations on the structures thus obtained were used to verify they were indeed stationary points and to determine zero-point energy, enthalpy, and entropy corrections to the electronic energies, thereby allowing free energies to be calculated. Wiberg bond indices were also calculated for the optimized structures using the Gaussian NBO Version 3.1 program [29]. Single-point solvation energies for the optimized structures using water as the solvent were computed using the IEF-PCM and CPCM implicit solvation methods [30, 31] as implemented in Gaussian 03. Final electronic energies were computed with single-point calculations on the optimized structures using the 6-311G(d,p) basis set (again with the exception of the Stuttgart effective core potential basis set on the metal center). Given the difference in standard-state concentrations in the gas phase (where the standard pressure of 1 atm equates to a concentration of 1/24.5 M from the ideal gas law) and in solution (1 M standard-state concentration), a translational entropy correction is included for the free energy changes computed in solution [32].

Formamide is used as the model substrate for the deformylation reaction to be catalyzed by the PDF biomimetic system. The reaction (Eq. 1) then yields ammonia as the deformylated peptide.



The high-spin state for the Fe^{II} -L coordination complexes here has been shown to be the ground state [19], and thus, all computations in the present work are for the high-spin state.

3 Results and discussion

3.1 Denticity of the $FeL(\text{formate})$ complexes

Two possible structures for the $FeL(\text{formate})$ product complex from the deformylation reaction were examined—one in which there is monodentate coordination of the formate

to the iron center and one in which the formate coordinate is bidentate. The denticity of the formate ligand is judged on the basis of iron–oxygen bond distances and Wiberg bond indices (with the former being less than 2.85 Å and the latter being greater than 0.10 to qualify as coordination between iron and oxygen) [19].

With any of the electron-withdrawing substituents or the H substituent ($\sigma_p \geq 0$), only the bidentate FeL(formate) structure was stable under optimization (Table 1). The electron-withdrawing ligand in these cases causes the iron center to become relatively electron deficient, which is counterbalanced by its coordinating more strongly with the anionic formate ligand. When electron-donating substituents are present, both monodentate and bidentate forms of FeL(formate) are stable structures, with the energetic preference between the two forms varying among the different electron-donating substituents.

3.2 Activation and reaction free energies for deformylation

Stationary points for the deformylation reaction were determined for the reaction as catalyzed by each of the 12 differently substituted ligands L. These points included the reactant FeL(OH) and product FeL(formate) complexes, as well as the transition state of the nucleophilic attack step and the resulting tetrahedral intermediate. The segment of the reaction coordinate connecting the tetrahedral intermediate to the FeL(formate) product complex was not modeled here. Experimental studies on the PDF enzyme have shown reaction rates to depend on the identity of the metal center [3, 10], leading to the conclusion that the proton transfer step(s) between the intermediate and product complexes are not rate-determining. These proton transfers are also mediated by amino acid residues in and near the active site of PDF [10], which are beyond the scope of the present biomimetic modeling study.

Computed reaction energetics—free energies of activation (ΔG^\ddagger), free energies of the intermediates versus the reactants (ΔG_{int}), and free energies of reaction (ΔG_{rxn})—with each of the 12 substituents are shown in Table 2. Free energies of activation range from 24.41 kcal/mol with the N=CHC₆H₅ substituent to 33.72 kcal/mol with the NO₂ substituent. Examination of the data here shows a general trend for activation energies to be highest when $|\sigma_p|$ is highest and lowest when $|\sigma_p|$ is lowest. ΔG_{int} trends similarly to the activation free energies, with each intermediate approximately 4–6 kcal/mol lower in energy than the corresponding transition state. Free energies of reaction range from a high of 3.06 kcal/mol with the NO₂ substituent to a low of –6.51 kcal/mol with the N=CHC₆H₅ substituent. A general trend toward lower ΔG_{rxn} values may be seen with lower σ_p parameters.

Table 1 Relative free energies for monodentate and bidentate FeL(formate) isomers with each substituent (in kcal/mol at 25 °C), computed as $\Delta G = G_{\text{bidentate}} - G_{\text{monodentate}}$

Substituent	σ_p	ΔG
NO ₂ ^a	0.78	bi
CN ^a	0.66	bi
CClF ₂ ^a	0.46	bi
F ^a	0.06	bi
H ^a	0.00	bi
<i>i</i> -Pr	–0.15	–2.65
CH ₃	–0.17	–1.01
OCH ₃	–0.27	3.17
OCH(CH ₃) ₂	–0.45	2.87
N=CHC ₆ H ₅	–0.55	0.30
NHCH ₃	–0.70	–2.44
N(CH ₃) ₂	–0.83	–2.97

$\Delta G < 0$ indicates bidentate is energetically preferred; $\Delta G > 0$, monodentate

^a Only bidentate coordination mode was stable under optimization

3.3 Reaction energetics analysis

In order to better understand the relationship between ΔG_{rxn} and ΔG^\ddagger and the Hammett parameters, Hammett plots using the Hammett σ_p parameters and reaction free energies and activation free energies (Figs. 3, 4, respectively) were made.² Based on the general trends just noted, a linear fit was used for the reaction free energies, while a quadratic fit was used for the activation free energies. The plots of ΔG_{rxn} and ΔG^\ddagger versus σ_p show good R^2 values of 0.767 and 0.596, respectively, for the current purpose of *qualitatively* understanding the effect of ligand substituents on the reaction energetics.

3.3.1 Reaction thermodynamics

The observed increase in ΔG_{rxn} with increase in the substituent σ_p value can be related to trends in the Fe–O bond orders for the hydroxide ligand in the reactant FeL(OH) complex and the formate ligand in the product FeL(formate) complex. As σ_p increases (i.e., the ligand substituent becomes more electron-withdrawing), this is correlated with an increase in the Fe–OH(hydroxyl) bond index (Fig. 5, Table S1), as the anionic hydroxyl ligand becomes more strongly bound to the iron center. This in

² The R=NHCH₃ point is omitted from the Hammett plot for ΔG_{rxn} (Fig. 3), while the R=N=CHC₆H₅ point is omitted from the Hammett plot for ΔG^\ddagger (Fig. 4). Based on an analysis of solvation energies, these two points are shown to be anomalous and therefore were not included in the reaction energetics analyses. See supporting information for detailed information on these points.

Table 2 Computed ΔG^\ddagger , ΔG_{int} , and ΔG_{rxn} for the deformylation reaction with each substituent (in kcal/mol at 25 °C)

Substituent	σ_p	ΔG^\ddagger	ΔG_{int}	ΔG_{rxn}
NO ₂	0.78	33.72	26.57	3.06
CN	0.66	30.37	25.12	0.68
CClF ₂	0.46	31.36	27.51	1.97
F	0.06	29.30	23.65	-0.81
H	0.00	29.31	25.51	0.17
<i>i</i> -Pr	-0.15	29.61	25.66	-1.94
CH ₃	-0.17	29.82	25.91	-0.74
OCH ₃	-0.27	30.43	25.20	-0.38
OCH(CH ₃) ₂	-0.45	31.64	26.44	-1.81
N=CHC ₆ H ₅	-0.55	24.41	19.90	-6.51
NHCH ₃	-0.70	32.08	28.23	1.21
N(CH ₃) ₂	-0.83	31.15	25.42	-5.66

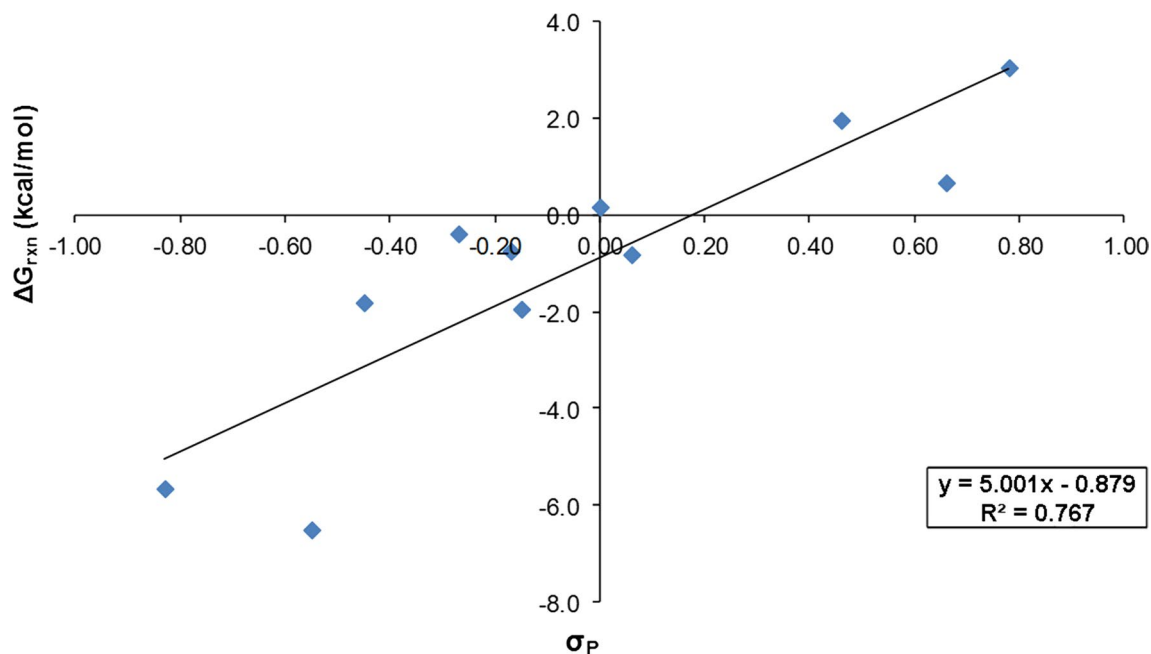
ΔG_{rxn} based upon lowest energy FeL(formate) isomer for each substituent

turn effectively lowers the energy of the reactant complex as the hydroxide ligand becomes less reactive and less nucleophilic [11]. With regards to the product FeL(formate) complex, increasing the substituent σ_p leads to an increase in the Fe–O(formate) bond index (Fig. 6, Table S1), as the anionic formate ligand becomes more strongly bound to the iron center. Similarly, this results in a more stable, lower energy FeL(formate) complex. The slopes for the linear regression lines in the Fe–OH(hydroxyl) and Fe–O(formate) bond indices versus σ_p plots (0.058 and

0.038, respectively), though, show that the effect on the Fe–O(hydroxyl) bond index is greater, and therefore, the effect on the reactant energy is greater as well. The reactant energy is lowered more than the product energy with more electron-withdrawing substituents, leading to an increase in ΔG_{rxn} as σ_p increases.

3.3.2 Reaction kinetics

The quadratic fit in the Hammett plot for the activation free energies and the positioning of the minimum in that plot near $\sigma_p \approx 0$ can likewise be understood through examination of the iron–oxygen bond orders in the reactant and transition state complexes. The positive correlation between σ_p and the Fe–OH(hydroxyl) bond index in the reactant complex implied a lowering in energy of the reactant complex as σ_p increased, and the hydroxide ligand became less reactive as a nucleophile. A positive correlation also exists between σ_p and the Fe–O (carbonyl oxygen in the formamide substrate) bond index in the transition state complex (Fig. 7, Table S1). More electron-withdrawing substituents lead to an increased iron–substrate interaction. The stronger ligation of the formamide carbonyl oxygen to the iron center (or, equivalently, increased Lewis acidity of the iron center) results in the carbonyl carbon becoming more electrophilic and therefore more activated toward nucleophilic attack, which has the effect of lowering the energy of the transition state. Thus, as σ_p increases, ΔG^\ddagger would increase as the reactant becomes more stable and decrease as the transition state becomes more stable. As σ_p decreases, ΔG^\ddagger

**Fig. 3** Plot of ΔG_{rxn} versus substituent σ_p value

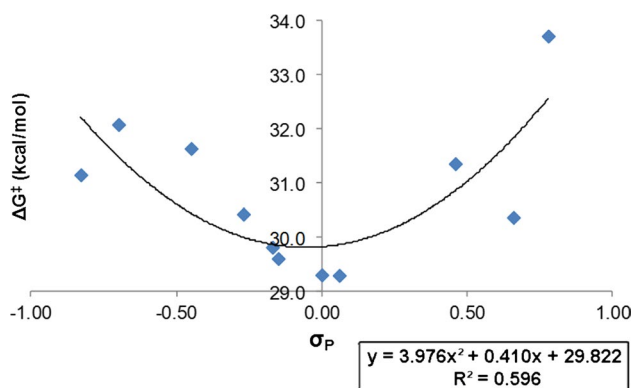


Fig. 4 Plot of ΔG^\ddagger versus substituent σ_p value

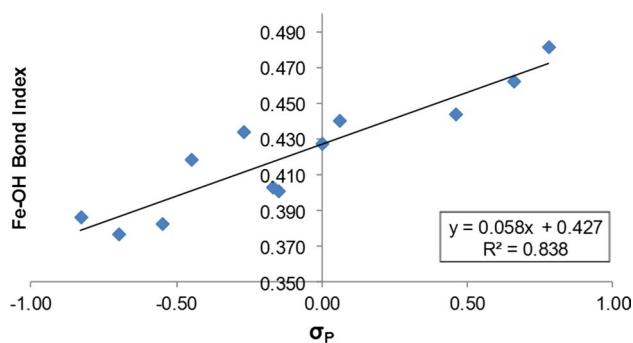


Fig. 5 Plot of Fe–OH bond index in the FeL(OH) reactant complex versus substituent σ_p value

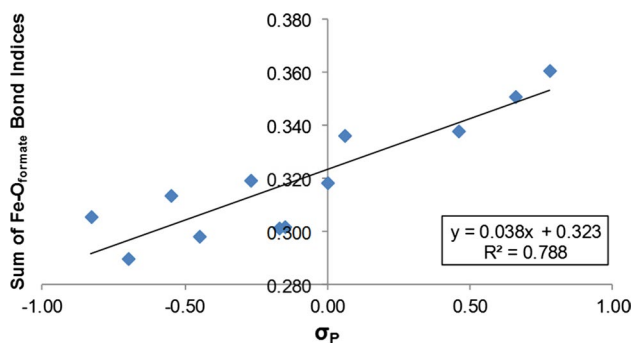


Fig. 6 Plot of the sum of Fe–O_{formate} bond indices in the FeL(formate) product complex versus substituent σ_p value

would decrease as the reactant becomes less stable and increase as the transition state becomes less stable. These offsetting effects on ΔG^\ddagger result in ΔG^\ddagger being a minimum as $|\sigma_p|$ becomes a minimum (i.e., near $\sigma_p \approx 0$).

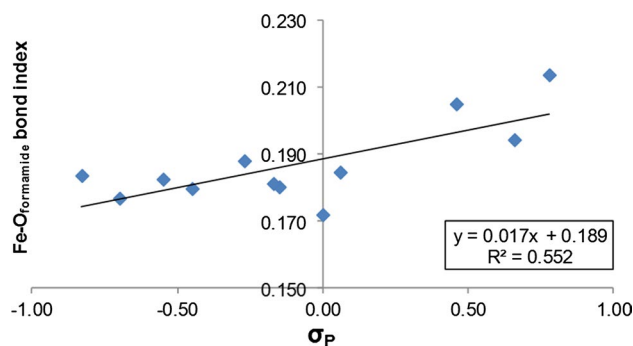


Fig. 7 Plot of Fe–O_{formamide} bond index in the transition state complex versus substituent σ_p value

4 Conclusions

The deformylation reaction catalyzed by PDF has been studied using a heteroscorpionate $N_2S_{thiolate}$ biomimetic ligand bound to an Fe^{II} metal center. Electron-donating and electron-withdrawing substituents were included on the biomimetic ligand in order to affect the electronic character of the model ligand system. DFT calculations were used to determine free energies of activation and reaction free energies in the presence of each substituent, as well as to characterize the ligand interactions with the Fe^{II} center through the reaction coordinate.

Deformylation becomes more thermodynamically favored as the substituent σ_p value decreases (i.e., as the substituent becomes more electron-donating). Both the hydroxide ligand in the FeL(OH) reactant complex and the formate ligand in the FeL(formate) product complex are more weakly bound to the Fe^{II} center with decreasing substituent σ_p . However, the former is found to be a more significant effect, allowing the hydroxide ligand to become a stronger nucleophile as substituents become more electron-donating and is responsible for the concurrent lowering of ΔG_{rxn} .

Deformylation is most kinetically favored as the substituent $|\sigma_p|$ decreases (i.e., neutral in terms of electron-withdrawal or electron-donation). Increasingly electron-donating substituents raise the energy of the reactant complex (and so lower the activation energy) by decreasing the Fe–OH bond order and increasing the nucleophilicity of the hydroxide ligand. At the same time, increasingly electron-donating substituents raise the energy of the transition state complex (and so raise the activation energy) by decreasing the Lewis acidity of the Fe^{II} metal center and therefore its ability to activate the substrate carbonyl group

for nucleophilic attack. The offsetting effects on the activation energy lead to a minimum in the activation energy near $|\sigma_p| \approx 0$.

Beyond providing new insight as to how ligand electronics can affect energetics during the deformylation reaction, the results here provide direction in the design of new biomimetic model systems for PDF that can be optimized for reaction thermodynamics and/or kinetics. Furthermore, the results here, when combined with potential future studies into the effect of the enzyme environment (e.g., hydrogen-bonding from residues near the active site [10]; general electrostatic or dispersion effects from residues near the active site) on active site electronics and energetics, constitute an important aspect of understanding how the peptide deformylase enzyme has been designed to optimize its catalytic efficiency.

Acknowledgments This work was funded by (a) California State University, Sacramento through the College of Natural Sciences and Mathematics and a Provost's Research Incentive Fund Grant and (b) a CSUPERB Faculty-Student Collaborative Research Seed Grant.

Conflict of interest The authors declare that they have no conflict of interest.

References

- Chan MK, Gong WM, Rajagopalan PTR, Hao B, Tsai CM, Pei DH (1997) *Biochemistry* 36:13904–13909
- Hao B, Gong WM, Rajagopalan PTR, Zhou Y, Pei DH, Chan MK (1999) *Biochemistry* 38:4712–4719
- Rajagopalan PTR, Yu XC, Pei DH (1997) *J Am Chem Soc* 119:12418–12419
- Yuan Z, White RJ (2006) *Biochem Pharmacol* 71:1042–1047
- Leeds JA, Dean CR (2006) *Curr Opin Pharmacol* 6:445–452
- Verma N, Kushwaha SP (2012) *Pharm Sci Monit* 3:2862–2874
- Verma SK, Jat RK, Nagar N, Saharan R, Sharma V, Pandey S, Bansal K (2011) *Pharmacophore* 2:114–123
- Winum J-Y, Kohler S, Scozzafava A, Montero J-L, Supuran CT (2008) *Anti-Infect Agents Med Chem* 7:169–179
- Giglione C, Pierre M, Meinnel T (2000) *Mol Microbiol* 36:1197–1205
- Becker A, Schlichting I, Kabsch W, Groche D, Schultz S, Wagner AFV (1998) *Nat Struct Biol* 5:1053–1058
- Yen N, Bogdanovic X, Palm G, Kuhl O, Hinrichs W (2010) *J Biol Inorg Chem* 15:195–201
- Leopoldini M, Russo N, Toscano M (2006) *J Phys Chem B* 110:1063–1072
- Wu X-H, Quan J-M, Wu Y-D (2007) *J Phys Chem B* 111:6236–6244
- Xiao C, Zhang Y (2007) *J Phys Chem B* 111:6229–6235
- Dong M, Liu H (2008) *J Phys Chem B* 112:10280–10290
- Groche D, Becker A, Schlichting I, Kabsch W, Schultz S, Wagner AFV (1998) *Biochem Biophys Res Commun* 246:342–346
- Lipscomb WN, Strater N (1996) *Chem Rev* 96:2375–2433
- Karambelkar VV, Xiao C, Zhang Y, Sarjeant AAN, Goldberg DP (2006) *Inorg Chem* 45:1409–1411
- Brown MF, Gherman BF (2011) *Theor Chem Acc* 128:137–146
- Jain RK, Hao B, Liu RP, Chan MK (2005) *J Am Chem Soc* 127:4558–4559
- Ragusa S, Blanquet S, Meinnel T (1998) *J Mol Biol* 280:515–523
- Hammes BS, Carrano CJ (2000) *J Chem Soc Dalton Trans* 3304–3309
- Hansch C, Leo A, Taft RW (1991) *Chem Rev* 91:165–195
- Gaussian 03, Revision D.01: Frisch MJ, Trucks GW, Schlegel HB, Scuseria GE, Robb MA, Cheeseman JR, J. A. Montgomery J, Vreven T, Kudin KN, Burant JC, Millam JM, Iyengar SS, Tomasi J, Barone V, Mennucci B, Cossi M, Scalmani G, Rega N, Petersson GA, Nakatsuji H, Hada M, Ehara M, Toyota K, Fukuda R, Hasegawa J, Ishida M, Nakajima T, Honda Y, Kitao O, Nakai H, Klene M, Li X, Knox JE, Hratchian HP, Cross JB, Bakken V, Adamo C, Jaramillo J, Gomperts R, Stratmann RE, Yazyev O, Austin AJ, Cammi R, Pomelli C, Ochterski JW, Ayala PY, Morokuma K, Voth GA, Salvador P, Dannenberg JJ, Zakrzewski VG, Dapprich S, Daniels AD, Strain MC, Farkas O, Malick DK, Rabuck AD, Raghavachari K, Foresman JB, Ortiz JV, Cui Q, Baboul AG, Clifford S, Cioslowski J, Stefanov BB, Liu G, Liashenko A, Piskorz P, Komaromi I, Martin RL, Fox DJ, Keith T, Al-Laham MA, Peng CY, Nanayakkara A, Challacombe M, Gill PMW, Johnson B, Chen W, Wong MW, Gonzalez C, Pople JA (2004) Gaussian, Inc., Wallingford, CT
- Lee CT, Yang WT, Parr RG (1988) *Phys Rev B* 37:785–789
- Handy NC, Cohen AJ (2001) *Mol Phys* 99:403–412
- Cohen AJ, Handy NC (2001) *Mol Phys* 99:607–615
- Dolg M, Wedig U, Stoll H, Preuss H (1987) *J Chem Phys* 86:866–872
- Gaussian NBO Version 3.1: Glendening ED, Badenhoop JK, Reed AE, Carpenter JE, Bohmann JA, Morales CM, Weinhold F (2001) Theoretical Chemistry Institute, University of Wisconsin, Madison <http://www.chem.wisc.edu/~nbo5>
- Tomasi J, Persico M (1994) *Chem Rev* 94:2027–2094
- Tomasi J, Mennucci B, Cammi R (2005) *Chem Rev* 105:2999–3094
- Cramer CJ (2004) *Essentials of computational chemistry: theories and models*, 2nd edn. Wiley, West Sussex